In-situ study of catalytic processes: Neutron diffraction of a methanol synthesis catalyst at industrially relevant pressure

Timur Kandemir,[a] Frank Girgsdies,[a] Thomas C. Hansen,[b] Klaus-Dieter Liss,[c] Igor Kasatkin,[a] Edward L. Kunkes,[a] Gregor Wowsnick,[a] Nikolas Jacobsen,[d] Robert Schlögl[a] and Malte Behrens[a]

a. Fritz-Haber-Institut der Max-Planck-Gesellschaft, Department of Inorganic Chemistry, Faradayweg 4-6, 14195 Berlin
Tel.: (+49) 30 8413-4408, E-mail: behrens@fhi-berlin.mpg.de

b. Diffraction Group, Institut Laue-Langevin, 38042 Grenoble

c. The Bragg-Institute, Australian Nuclear Science and Technology Organisation, Lucas Heights, NSW 2234

d. BU Catalysis & Energy of Clariant Produkte (Deutschland) GmbH (formerly Süd-Chemie), 83052 Bruckmühl

Heterogeneous catalysts are dynamic materials that interact with the gas phase present in catalytic reactions. Changes that may occur when a catalyst is in contact with reactive molecules comprise adsorbate-induced surface reconstruction,[1] surface segregation,[2] inclusion of foreign atoms from the gas phase into the sub-surface[3] and compound formation in the bulk such as oxide,[4] hydride,[3] carbide[5] or nitride[6] formation of a metal catalyst. These modifications will affect the catalytic properties and depend on the chemical potential of the gas phase species. An extrapolation of experimental results obtained at low pressure to pressure regimes of industrial relevance is often not straightforward ("pressure gap"[7]). To better understand the impact of dynamic catalyst changes, application of in situ techniques[8] working at industrially relevant conditions is desirable. Here, we report on the potential of neutron diffraction (ND) as a tool for in situ analysis of heterogeneous catalysts. ND studies have been carried out on many inorganic materials in various sample environments.[9] Pioneering in situ ND studies of catalysts has been performed by Turner et al.[10] and Walton et al.[11] Inelastic neutron scattering was used for catalyst characterization, e.g., by the groups of Albers, Lennon and Parker.[12]

Similar to in situ XRD,[13] ND is complementary to other in situ techniques used in catalysis research, such as ambient pressure XPS,[14] XAFS[15] or Raman spectroscopy.[16] It is uniquely suitable for in situ-studies in thick-walled metallic tubular reactors which allow application of realistic reaction conditions. No special pressure-tight windows or complex reactor design is required, if a wall material is chosen that shows only minor absorption of neutrons and thus allows sufficient penetration through the walls.[17] ND is a bulk-sensitive method that gives quantitative, average structural (lattice parameter) and microstructural (domain size, lattice strain, defects) information. In contrast to XRD, the scattering power is independent of the diffraction angle providing diffraction peaks at higher angles with higher intensity. This is in particular useful for the investigation of nanomaterials with highly symmetric crystal structures that often suffer from few and weak XRD peaks available for structural analysis. Figure 1 compares ex-situ ND with XRD data and shows a TEM image of the Cu/ZnO/Al$_2$O$_3$ catalyst used in this study.

Such catalysts are employed for the industrial synthesis of methanol from syngas (H$_2$/CO/CO$_2$). While being used today mainly as a base chemical and a feedstock for chemical industry, methanol has interesting potential as a sustainable synthetic fuel in a future energy scenario[18] if produced from anthropogenic CO$_2$ and regenerative H$_2$. The exothermic methanol formation is favoured at low T and high P. In the industrial process it is conducted at $T = 493 - 573$ K and $P = 3.5 - 10$ MPa.[19]

The nature of the active sites of Cu/ZnO/Al$_2$O$_3$ catalysts and of the often observed "Cu-ZnO synergy" has been vividly debated.[19b] For instance, a model emphasizing the role of defects found in the active Cu phase after the industrially applied synthesis[20] seems in apparent contradiction to a model focusing on the dynamic interaction of Cu and ZnO leading to dynamic morphology changes of the Cu particles.[21] The latter was related to metal-support interaction and observed on supported model catalysts. Due to the high mobility of Cu according to this model, annealing of structural defects can be expected under working conditions. Based on a structure-activity correlation and DFT calculations, we have recently presented a model for the active site of methanol synthesis that combines both views.[22] Planar defects have been shown to lead to changes in surface faceting of the Cu nanoparticles associated with formation of steps and kinks that represent high energy surface sites of special catalytic activity. For a series of Cu/ZnO-based catalysts a linear correlation of the defect concentration with the intrinsic activity of the exposed Cu surface was observed. In addition, surface decoration[21a] of Cu with ZnO$_x$ by strong metal support interaction[23] (SMSI) has been confirmed by HRTEM and in situ-XPS on a high-performance catalyst.[22]

Hence, ZnO rather than Cu seems to be the mobile component in course of Cu-ZnO interaction, thus enabling dynamic changes and a static Cu defect structure at the same time. The predominating planar defects in the Cu particles are twin boundaries and stacking faults that can be observed in TEM images (Fig. 1b) and quantitatively studied with diffraction techniques.

In the present study, an industrial Cu/ZnO/Al$_2$O$_3$ catalyst with similar properties as the materials presented in ref. [20] has been used for methanol synthesis and its microstructure has been studied near industrial working conditions using in situ ND. A typical syngas mixture was applied at 523 K and 6 MPa in a continuous flow reactor, which was described in detail elsewhere.[17] Catalytic activity studies in the laboratory at differential conditions confirmed stable methanol productivity in the range reported for state-of-the-art Cu/ZnO/Al$_2$O$_3$ catalysts. During the ND experiment the reaction was in thermodynamic equilibrium simulating the chemical potentials of the gas phase in an

industrial reactor near the very end of the catalyst bed and in the outlet. At the same time, equilibrium guarantees a largely homogeneous and gradient-free catalyst bed for ND studies. Analogous in situ diffraction studies were carried out in a high-flux experiment with a time resolution of 5 min (ILL, Grenoble, France)[24] and in a high instrumental resolution experiment (Bragg Institute, Lucas Heights, Australia).[25] The catalyst was reduced in a D_2 stream in the reactor prior to the catalytic reaction. During the in situ study, methanol was detected at the outlet of the reactor by mass spectrometry. Figure 2 shows the high-resolution neutron diffraction patterns of the reduced catalyst in 0.1 MPa Ar at 523 K right before the synthesis and during synthesis under 6 MPa of syngas after 3 and 24 h time-on-stream (TOS).
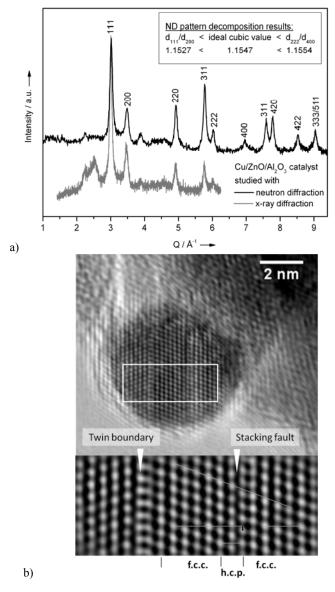

a)

b)

Figure 1. a) Diffraction pattern of the fresh Cu/Zn/Al$_2$O$_3$ catalyst aquried at room temperature with ND (black pattern) and laboratory XRD (Cu K , grey pattern). Peaks due to Cu are indexed. Due to different wavelenghts used, the abscissa is given in reciprocal space. b) High-resolution TEM image of a typical ellipsoidal copper particle in the used catalyst. Planar defects and the resulting thin hcp domain are marked in the close-up.

The Rietveld-fit of the fresh catalyst in Ar (Fig. 2, top) reveals the presence of fcc-Cu as the major phase with a unit cell length of $a = 3.6268$ ($\pm$ 0.0008) Å at 523 K (more results of the Rietveld analysis are presented as supporting information). Additional weaker peaks of the catalyst are due to the ZnO component (green profile). No major changes of the Cu phase are obvious from a first comparison of the three ND patterns recorded at different conditions and the lattice parameter of Cu does not vary significantly. Thus, bulk inclusion of C or H species from the gas phase in the Cu lattice of working catalysts can be readily excluded. Only a slight sharpening of the Cu peaks can be detected, which corresponds to an increase in crystalline domain size from 5.9 ($\pm$ 0.1) nm to 6.4 ($\pm$ 0.1) nm with time and is due to sintering of the Cu particles, which is a relevant deactivation mechanism of methanol synthesis catalysts.[26]
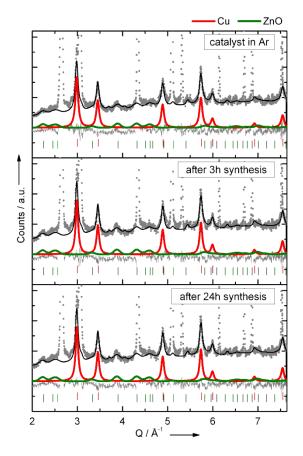
Figure 2. Rietveld-fits of the catalyst before (0.1 MPa Ar, upper panel), at the beginning (center) and after 24 hours of methanol synthesis (bottom) at 523 K and 6 MPa. Experimental data is shown in grey, the calculated pattern of the catalyst as black line. The thin grey line is the difference between experimental and calculated pattern. The contribution of the Cu phase and ZnO is marked as red and green lines with tick marks at the positions of Bragg reflections. Additional strong peaks due to the Al reactor wall were treated as peak-phase during Rietveld-analysis and are excluded from the overall calculated profile shown here.

Planar defects have been observed in a comparative TEM and XRD study of similar $Cu/ZnO/Al_2O_3$ catalysts.[20] Such defects are expected to contribute to the anisotropic broadening of the ND peaks, but line profile analysis turned out to be complex and data analysis suffered from the nanostructured nature of the samples and the in situ conditions (for details see supporting information). However, application of a pattern decomposition method has been shown[22] to allow qualitative confirmation of the presence of stacking faults in the Cu nanoparticles. This evaluation is based on the peak positions, which can be determined with higher precision compared to the other peak profile parameters.

An ideal defect-free Cu is expected to show a ratio of the distances between the (111) and (200) lattice planes of $2/\sqrt{3} = 1.1547$. The presence of stacking faults causes a shift of the 111 and 200 peaks towards each other and lowers this ratio.[27] Careful evaluation of the peak positions of the ex-situ ND data shown in Figure 1a revealed that such a shift is also found for the catalyst under study here. Additionally, a consistent opposite shift of the 222 and 400 reflection pair was observed too (Fig. 1a, inset), which also confirms the presence of stacking faults. Furthermore, HRTEM observations provide further evidence for this type of planar defects in the catalyst as shown in Figure 1b. The resulting deviation from cubic symmetry can be used as a measure for the stacking fault probability α. Based on the lower order reflection pair, that exhibits well-defined peaks even in the in-situ ND data, α is calculated according to $\alpha = 8.3 \times [(2/\sqrt{3}) - (d_{111}/d_{200})]$.[27] Figure 3 shows the evolution of d_{111}/d_{200} of the Cu catalyst versus TOS during methanol synthesis.

Similar values are obtained in both the high-flux and the high-resolution experiments that are significantly lower than that observed for a macrocrystalline Cu reference powder measured in the same reactor tube. It is noted that the experimental values of this defect-poor reference deviate from the theoretical value expected for a perfect fcc lattice in both experiment (cf. right hand axis in Fig. 3b). This is attributed to systematic displacement errors of the complex in situ cell at the beamline, which will lead to an offset-like effect in d_{111}/d_{200} and also causes the slight difference of this parameter obtained from ex-situ and in-situ data of the same catalyst as seen in Figure 1a and 3. Thus, in contrast to previously reported ex situ ND data,[22] α is evaluated in a semi-quantitatively fashion in this study and only the consistent internal trends observed during the two in situ experiments are discussed in the following. However, it is noted that the magnitude of deviation between catalyst and reference on the α-scale corresponds to a few %, which is in agreement with previous studies of similar materials.[20, 22]

These results confirm that the Cu phase in the active catalyst bears stacking faults. Furthermore, this data proves that the planar defects in the Cu nanoparticles are relatively stable under working conditions and do not disappear when switching from Ar to syngas on a time scale proposed for Cu morphology changes (< 30 min[21c]), but resist for 24 hours TOS. Annealing of the defects would lead to an approach toward the reference value, which is in both experiments hardly significant in the investigated time interval.

Figure 3 reveals that the difference between the catalytically active copper phase and a bulk reference copper material, that has been observed before[20] and ascribed to the peculiar microstructure of the former,[28] is mostly conserved under working conditions. This finding supports the concept of a rather static Cu bulk phase, which maintains its defect structure. It is noted that no conclusion on dynamic surface behaviour like surface diffusion, surface reconstruction or re-crystallization can be made based on these results obtained by a bulk diffraction method. Such surface mobility (and an effect of the gas atmosphere on it) seems even very likely considering the low Hüttig temperature of Cu and the beginning sintering of the nanoparticles observed in the experiment.
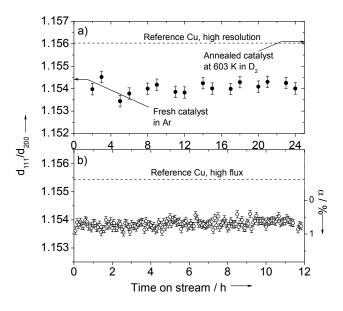

Figure 3. d_{111}/d_{200} ratio of Cu in the catalyst and reference sample over TOS during methanol synthesis under industrially relevant conditions in the high resolution- (a) and high flux-experiments (b). This ratio is a measure for the defectiveness of Cu (see text). The formally resulting stacking fault concentration is shown on the right axis of (b). The error bars are the standard deviations of the two datasets neglecting systematic errors due to, e.g., wavelength and zero-shift.
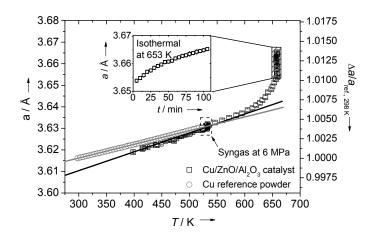

Figure 4. Evolution of the lattice parameter of Cu in the Cu/ZnO/Al$_2$O$_3$ catalyst and of the Cu reference powder with temperature. The Cu powder was heated in Ar at 0.1 MPa, while the calcined catalyst was heated to 523 K in D$_2$ (0.1 MPa), then subjected to 12 hours of methanol synthesis at 523 K in the syngas feed (6 MPa) and finally heated in D$_2$ (0.1 MPa) to 653 K. Heating rate was 1 K/min and one ND pattern corresponds to ca. 5 K. The dashed square at 523 K marks the period of 12 h synthesis. The right axis shows the lattice expansion relative to the reference at 298 K.

However, the bulk stability of the Cu particles, suggest that the observed strong interactions between Cu and ZnO[22] manifest themselves rather in form of mobile ZnO$_x$ than mobile Cu in the industrial high performance catalyst. The material under study here exhibits relatively large Cu nanoparticles and poorly crystalline ZnO and the observations are not necessarily in contradiction with previous reports of a mobile Cu phase and static ZnO, which were made on highly crystalline ZnO decorated with very small Cu particles,[21] as such differences might be able to cause to a switch of the mobile component during SMSI-induced dynamics.

To study the response of the catalyst to higher *T* than applied for methanol synthesis, the sample has been heated after the 24 h TOS experiment in D$_2$ atmosphere to 603 K (high resolution experiment) and 653 K (high-flux experiment). This is beyond the temperature limit of approximately 573 K, which should not be exceeded in methanol synthesis to suppress activity loss due to sintering.[26a] At 603 K the Cu

crystallites have grown significantly to 9.4 (±0.2) nm as revealed by ND peak width analysis. At the same time, also the defects have been annealed and α is at the same level as the bulk reference (Fig. 3a) showing the strong effect of temperature on the bulk mobility of the Cu particles by approaching the Tammann temperature. According to a simple estimation, bulk re-crystallization is expected to start at 0.5 T_M, which in case of Cu is at 679 K.

The evolution of the Cu lattice parameter over the full *T*-range is shown in Figure 4 (high flux data). The thermal expansion of the reference Cu powder as well as of the catalyst is linear at $T < 523$ K. Interestingly, the lattice parameters at room temperature as well as the thermal expansion coefficient of catalyst and reference differ. The extrapolated Cu lattice parameter is 3.6114 (± 0.0009) Å for the catalysts and thus 0.1% smaller than that of the bulk reference, which corresponds to the literature value. The slightly lower value for the catalyst is in agreement with ex situ results[22] and ascribed to the complex microstructure of the composite catalyst. Lattice contraction might be due to the lower particles size as observed for many metals[29] or to the effect of defects. However, since the metal particles in this catalyst are relatively large and the effect of stacking faults on the average lattice parameter is low, the most likely explanation is the interfacial contact with the oxide phase. Also different thermal expansion coefficients have been previously observed for nanomaterials compared to their bulk counterparts[30] and are probably also influenced by the contact to the oxide phase and the presence of defects.

It can be seen in Figure 4 that the period of methanol synthesis over 12 hours (dashed square) did not lead to any lattice expansion. Thus the beginning formation of α-brass in the bulk of the Cu particles by partial reduction of the ZnO component can be safely excluded during methanol synthesis under industrial conditions. Spencer[31] reported a low diffusion coefficient of zinc in copper at methanol synthesis condition of 523 K that increased when going to 623 K. Accordingly, brass formation is observed at higher *T* in D_2 and causes a deviation from the linear behaviour starting at around 603 K. In this *T*-regime, thermal expansion is superimposed to the lattice expansion due to successive substitution of Cu by larger Zn atoms in the newly formed alloy as is evidenced by the continuing lattice expansion in the isothermal regime at 653 K (Fig. 4, inset). Based on the results of Grazzi et al.,[32] the concentration of Zn in the alloy can be estimated to 4.88 (± 0.05) mass-% after 100 minutes of isothermal treatment at 653 K in 0.1 MPa D_2.

In summary, the potential of in situ ND to study solid catalysts in a realistic reactor at high pressure conditions that are relevant for applications has been demonstrated for a $Cu/ZnO/Al_2O_3$ methanol synthesis catalyst. The metallic Cu component is nanostructured and highly defective. The deviation from ideal bulk-Cu is manifested in a lattice contraction at room temperature and an increased thermal expansion coefficient. In addition, a high concentration of stacking faults has been detected in the Cu nanoparticles. These bulk defects were shown to be stable upon changing the gas atmosphere to partial pressures as applied in industrial methanol synthesis. Also, the bulk inclusion of reactive species from the gas phase as well as the formation of brass during methanol synthesis can be excluded. The latter alloying as well as the annealing of the bulk defects was observed only at significantly higher *T* than used in the industrial process. Under reaction conditions, the bulk integrity of the nanoparticles as well as the non-ideal nature of Cu was found to be relatively stable in industrial catalysts. Thus, the results suggest that the interaction between metal and oxide during methanol synthesis involves dynamics of the poorly crystalline ZnO component rather than of the whole bulk of the Cu particles and affect only the Cu surface.

Future work using this methodology will aim at correlation of the described structural properties with catalytic performance and include information about the evolution of the microstructure with deactivation of the catalyst over a longer TOS.

Experimental Section

The catalyst was provided by Clariant Produkte (Deutschland) GmbH. The methanol synthesis reaction was done at 523 K and 6 MPa in thermodynamic equilibrium with a syngas mixture (CO_2:CO:D_2:Ar = 8:6:75:6) in a flow cell described previously.[17] Diffraction experiments were carried out on D1B (ILL, Grenoble, F)[24a] and on ECHIDNA (ANSTO, Lucas Heights, AUS).[25] Sieve fractions of the catalyst and the polycrystalline Cu reference (99,8%, Heraeus) were used (200–300 μm). Rietveld refinement was done with the Topas 4.2 software. Multiple peak fitting during pattern decomposition was carried out with OriginPro 8.5 peak analyzer. For more experimental details, please refer to the supporting information.

References

[1]   a)K. Christmann, F. Chehab, V. Penka, G. Ertl, *Surface Science* **1985**, *152-153, Part 1*, 356; b)G. A. Somorjai, M. A. Van Hove, *Progress in Surface Science* **1989**, *30*, 201.

[2]   a)K. J. J. Mayrhofer, V. Juhart, K. Hartl, M. Hanzlik, M. Arenz, *Angewandte Chemie-International Edition* **2009**, *48*, 3529; b)P. Strasser, S. Koh, T. Anniyev, J. Greeley, K. More, C. F. Yu, Z. C. Liu, S. Kaya, D. Nordlund, H. Ogasawara, M. F. Toney, A. Nilsson, *Nature Chemistry* **2010**, *2*, 454.

[3]   D. Teschner, J. n. Borsodi, Z. n. Kis, L. s. Szentmiklósi, Z. Révay, A. Knop-Gericke, R. Schlögl, D. Torres, P. Sautet, *The Journal of Physical Chemistry C* **2010**, *114*, 2293.

[4]   G. R. Patzke, Y. Zhou, R. Kontic, F. Conrad, *Angewandte Chemie International Edition* **2011**, *50*, 826.

[5]   J. W. Niemantsverdriet, A. M. Van der Kraan, W. L. Van Dijk, H. S. Van der Baan, *The Journal of Physical Chemistry* **1980**, *84*, 3363.

[6]   B. Herzog, D. Herein, R. Schlögl, *Applied Catalysis A: General* **1996**, *141*, 71.

[7]   a)J. A. Dumesic, G. W. Huber, M. Boudart, in *Handbook of Heterogeneous Catalysis*, Wiley-VCH Verlag GmbH & Co. KGaA, **2008**; b)M. Havecker, A. Knop-Gericke, T. Schedel-Niedrig, R. Schlogl, *Angewandte Chemie-International Edition* **1998**, *37*, 1939.

[8]   a)B. Weckhuysen, *In Situ Spectroscopy of Catalysts: X-ray diffraction and scattering* Amercian Scientific Publishers, **2004**; b)A. Brückner, *Catalysis Reviews* **2003**, *45*, 97.

[9]   I. F. Bailey, *Zeitschrift für Kristallographie* **2003**, *218*, 84.

[10]   J. F. C. Turner, R. Done, J. Dreyer, W. I. F. David, C. R. A. Catlow, *Review of Scientific Instruments* **1999**, *70*, 2325.

[11]   R. I. Walton, R. J. Francis, P. S. Halasyamani, D. O' Hare, R. I. Smith, R. Done, R. J. Humphreys, *Review of Scientific Instruments* **1999**, *70*, 3391.

[12]   a)D. Lennon, D. T. Lundie, S. D. Jackson, G. J. Kelly, S. F. Parker, *Langmuir* **2002**, *18*, 4667; b)A. R. McInroy, D. T. Lundie, J. M. Winfield, C. C. Dudman, P. Jones, S. F. Parker, J. W. Taylor, D. Lennon, *Physical Chemistry Chemical Physics* **2005**, *7*, 3093; c)A. R. McInroy, D. T. Lundie, J. M. Winfield, C. C. Dudman, P. Jones, S. F. Parker, D. Lennon, *Catalysis Today* **2006**, *114*, 403; d)S. F. Parker, J. W. Taylor, P. Albers, M. Lopez, G. Sextl, D. Lennon, A. R. McInroy, I. W. Sutherland, *Vibrational Spectroscopy* **2004**, *35*, 179; e)P. W. Albers, S. F. Parker, (Eds.: L. Liang, R. Rinaldi, H. Schober), Springer US, **2009**, pp. 391.

[13]   R. Schlogl, *Advances in Catalysis, Vol 52* **2009**, *52*, 273.

[14]   M. Salmeron, R. Schlogl, *Surface Science Reports* **2008**, *63*, 169.

[15]   J. D. Grunwaldt, B. S. Clausen, *Topics in Catalysis* **2002**, *18*, 37.

[16]   I. Wachs, *Topics in Catalysis* **1999**, *8*, 57.

[17]   T. Kandemir, D. Wallacher, T. Hansen, K.-D. Liss, R. Naumann d'Alnoncourt, R. Schlögl, M. Behrens, *Nuclear Instruments and Methods in Physics Research Section A: Accelerators, Spectrometers, Detectors and Associated Equipment* **2012**, *673*, 51.

[18]   G. A. Olah, A. Goeppert, G. K. S. Prakash, *Beyond oil and gas : the methanol economy*, Wiley-VCH, Weinheim an der Bergstrasse, Germany, **2006**.

[19]   a)E. Fiedler, G. Grossmann, D. B. Kersebohm, G. Weiss, C. Witte, in *Ullmann's Engcylopedia of Industrial Chemistry*, Weily-VCH Weihneim, **2011**; b)J. B. Hansen, P. E. Højlund Nielsen, in *Handbook of Heterogeneous Catalysis*, Wiley-VCH Verlag GmbH & Co. KGaA, **2008**.

[20]   I. Kasatkin, P. Kurr, B. Kniep, A. Trunschke, R. Schlogl, *Angewandte Chemie-International Edition* **2007**, *46*, 7324.

[21]   a)J. D. Grunwaldt, A. M. Molenbroek, N. Y. Topsoe, H. Topsoe, B. S. Clausen, *Journal of Catalysis* **2000**, *194*, 452; b)P. L. Hansen, J. B. Wagner, S. Helveg, J. R. Rostrup-Nielsen, B. S. Clausen, H. Topsoe, *Science* **2002**, *295*, 2053; c)P. C. K. Vesborg, I. Chorkendorff, I. Knudsen, O. Balmes, J. Nerlov, A. M. Molenbroek, B. S. Clausen, S. Helveg, *Journal of Catalysis* **2009**, *262*, 65.

[22]   M. Behrens, F. Studt, I. Kasatkin, S. Kühl, M. Havecker, F. Abild-Pdersen, S. Zander, F. Girgsdies, P. Kurr, B. Kniep, M. Tovar, R. W. Fischer, J. K. Norskov, R. Schlogl, *Science* **2012**.

[23]   R. N. d'Alnoncourt, X. Xia, J. Strunk, E. Loffler, O. Hinrichsen, M. Muhler, *Physical Chemistry Chemical Physics* **2006**, *8*, 1525.

[24]   a)I. P. Orench, J. A. R. Velamazán, J. Campo, *Neutron News* **2010**, *21*, 20; b)R. Allemand, J. Bourdel, E. Roudaut, P. Convert, K. Ibel, J. Jacobe, J. P. Cotton, B. Farnoux, *Nuclear Instruments and Methods* **1975**, *126*, 29.

[25]   K.-D. Liss, B. Hunter, M. Hagen, T. Noakes, S. Kennedy, *Physica B: Condensed Matter* **2006**, *385–386, Part 2*, 1010.

[26]   a)M. V. Twigg, M. S. Spencer, *Topics in Catalysis* **2003**, *22*, 191; b)G. Prieto, J. Zečević, H. Friedrich, K. P. de Jong, P. E. de Jongh, *Nat Mater* **2013**, *12*, 34.

[27]   B. E. Warren, *Progress in Metal Physics* **1959**, *8*, 147.

[28]   M. M. Gunter, T. Ressler, B. Bems, C. Buscher, T. Genger, O. Hinrichsen, M. Muhler, R. Schlogl, *Catalysis Letters* **2001**, *71*, 37.

[29]   a)R. Lamber, S. Wetjen, N. I. Jaeger, *Physical Review B* **1995**, *51*, 10968; b)Z. Huang, P. Thomson, S. Di, *Journal of Physics and Chemistry of Solids* **2007**, *68*, 530.

[30]   a)J. Hu, W. Cai, C. Li, Y. Gan, L. Chen, *Applied Physics Letters* **2005**, *86*, 151915; b)A. Plech, V. Kotaidis, S. Grésillon, C. Dahmen, G. von Plessen, *Physical Review B* **2004**, *70*, 195423.

[31]   M. S. Spencer, *Surface Science* **1987**, *192*, 329.

[32]   F. Grazzi, L. Bartoli, S. Siano, M. Zoppi, *Analytical and Bioanalytical Chemistry* **2010**, *397*, 2501.

Supporting information

In-situ study of catalytic processes at high temperatures: Neutron diffraction of a methanol synthesis catalyst under industrial conditions

Timur Kandemir, Frank Girgsdies, Thomas C. Hansen, Klaus-Dieter Liss, Edward L. Kunkes, Gregor Wowsnick, Nikolas Jacobsen, Robert Schlögl and Malte Behrens*

* behrens@fhi-berlin.mpg.de

Content

Sample preparation and catalytic experiments

Approx. 6g of the catalyst precursor $CuO/ZnO/Al_2O_3$ were loaded into the flow cell.[S1] Reduction of the catalyst was carried out under a flow of 100 Nml/min pure D_2 at 1 atm, while the heating rate was 1 K/min up to 523 K. Afterwards, the feed was changed to Ar to acquire a diffraction pattern of the activated catalyst before methanol synthesis. On the ILL-experiment, methanol synthesis was carried out for 12 h under 6 MPa syngas ($CO_2:CO:D_2:Ar$ = 8:6:75:6) at thermodynamic equilibrium with a flow of 167 Nml/min, on the ANSTO experiment for 24 h under the same conditions. After 12 h of synthesis at ILL, the feed was switched to D_2 (1 atm) again and the catalyst bed was heated to 653 K with a heating rate of 5 K/min. After reaching the final temperature, the sample was kept isothermally for 100 min. After the 24 h of methanol synthesis at ANSTO, the catalyst bed was purged with Ar (1 atm) to acquire a pattern after synthesis. Afterwards, the bed was heated up in D_2 (1 atm) to 603 K, and kept at that temperature for additional 12 h. After that time, a pattern of the annealed sample was recorded. As a reference, polycrystalline Cu powder was heated from RT to 523 K in Ar with a heating rate of 1 K/min in the same setup.

Neutron beamline configurations

High-flux experiments
At ILL the beamline D1B was used. While requesting the highest available neutron flux for a sufficient time resolution of the experiment, a focusing, highly oriented pyrolitic graphite monochromator was used to select a wavelength of λ=2.52346 ±0.000129 Å (refined using a $Na_2Ca_3Al_2F_{14}$ standard), which led to an effective flux of 6.5×10^6 n cm^{-2}s^{-1} at the sample. By setting the ^{3}He/Xe position-sensitive detector[S2] to a take-off angle of 45° the angular range up to 125° 2θ (corresponding Q-range 1.91 Å^{-1} to 4.42 Å^{-1}) was covered. While having the highest possible flux on the instrument, the average acquisition time per pattern was 5 min.
High-resolution experiments
The ECHIDNA-diffractometer used at ANSTO was designed for collecting high-resolution powder diffraction data. The Ge (335) monochromator provides a wavelength λ=1.62275 ±0.0000203 Å (refined using a LaB_6 standard). A large array of 128 Position-sensitive ^{3}He detectors enables access to an angular range of 4° to 164° in 2θ (corresponding Q-range 0.28 Å^{-1} to 7.7 Å^{-1}). While the instrument configuration was set to reach a resolution of $\Delta d/d \sim 5 \times 10^{-4}$ the average acquisition time per pattern was 1 h or 2 h. More specifications about the beamline could be found in ref. [S3].

Data evaluation procedures and selected results

Rietveld refinement of neutron diffraction patterns
As a first step Rietveld refinements of the neutron diffraction patterns were done in the range 15–160° 2θ (corresponding to 0.2736 Å^{-1} to 7.6655 Å^{-1}) using the software package TOPAS 4.2 as shown Figure 1 of the main paper. The background was modeled using a forth order Chebychev-polynomial. The neutron wavelength was refined with a NIST LaB$_6$ standard sample (SRM 660a) (instrument data file: ECH0005658, FHI database entry number: ID550625) to 1.62275 (±0.00000203) Å and fixed during the refinements of the catalyst sample. Some technical details and selected results of the refinements are listed in Tables S1 and S2, respectively. This analysis was performed on the catalyst in Ar before synthesis (ECH0005667, ID550634), after 3 h synthesis under synthesis conditions (ECH0005669, ID550636), after 24 h under synthesis conditions (ECH0005683, ID550651), of the Cu-refence (ECH0005657, ID550624) and the sintered catalyst (ECH0005693, ID550661).

Table S1: Details of the Rietveld refined of the diffraction pattern from Figure 1, the Cu reference poweder and the sintered catalyst.

Sample	R$_{Bragg}$	R$_{wp}$ / R$_{wp}$'	No. of parameters	GOF
ID550634 (in Ar)	2.288	7.7720/14.9093	12	1.8735
ID550636 (3h TOS)	1.9540	6.9444/14.0034	12	1.7323
ID550651 (24h TOS)	1.7091	6.8830/13.5405	12	1.8572
ID550624 (Cu ref.)	2.2190	10.2898/14.4877	8	2.7984
ID550661 (sintered)	2.2971	7.2761/14.0739	14	2.6878

Table S2: Selected results of the Rietveld-refinement

Sample	Lattice parameter a /Å	Cu wt% Rietveld	B$_{eq}$ / Å^2	Lvol-IB^a / nm	Zero shift / ° 2θ
ID550625 (LaB$_6$)	4.1569 ±9.7x10^{-8}	0	-	-	-0.1046 ±0.0002
ID550634 (in Ar)	3.62675 ±0.000799	74.065 ±1.401	1.089 ±0.08	5.430 ±0.131	-0.3427 ±0.0188
ID550636 (3h TOS)	3.62710 ±0.000699	70.574 ±1.315	0.9816 ±0.07	5.892 ±0.133	-0.2725 ±0.0166
ID550651 (24h TOS)	3.62805 ±0.000608	71.174 ±1.152	0.9537 ±0.06	6.380 ±0.127	-0.2705 ±0.0143
ID550624 (Cu ref.)	3.61495 ±0.000076	100	0.6206 ±0.01	72.074 ±7.025	0.1808 ±0.0118
ID550661 (sintered)	3.63502 ±0.000594	70.652 ±1.117	1.064 ±0.07	9.434 ±0.188	-0.3485 ±0.0137

Pattern Decomposition with single peak fit method
For Fig. 2b and 3 of the main paper, the time resolved neutron diffraction pattern from the high-flux measurement at the ILL were fitted by the single peak pattern decomposition method. The 111 and 200 peaks of Cu were fitted with a pseudo-Voigt 1 peak shape function and a third order polynomial background function in OriginPro 8.5.0G®. The ratio of the overlapping scattering intensities of the Cu-Peaks with the Al peaks of the reactor walls were estimated by measurements of the "empty can" at RT, 523 K and 603 K. During the fit of the Cu peaks the center, FWHM as well as the profile shape factor of the overlapping Al-Peaks were kept constant to achieve the least-squares minimum amplitude of the overlapping scattering intensities. The graphical result of the pattern decomposition of the Cu and Al peaks is shown in Fig. S1.
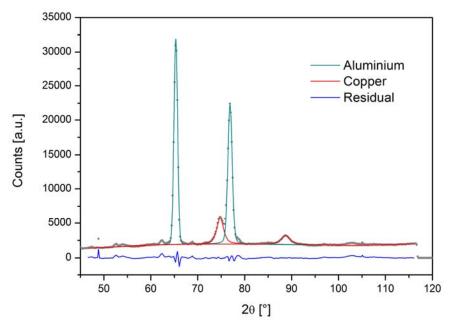
Figure S1: Schematic pattern decomposition on high-flux diffraction data measured on D1B at ILL. The fitted peak centers of the Cu 111 and 200 peaks at approximately 75 and 89 °2θ were used for further evaluation.

To obtain the d-spacings of (111) and (200) shown in Fig. 2b, the wavelength determined for the $Na_2Ca_3Al_2F_{14}$ standard (089127, ID529386)[S4] was used in Bragg's equation and the raw peak positions were corrected by the zero-shift value resulting from the standard pattern refinement (0.97758 ±0.0052 °2θ). The Cu lattice parameter shown in Fig. 3 has been determined accordingly from the position of the 111 peak.

The high-resolution data recorded at ECHIDNA was treated accordingly to obtain the data set shown in Fig. 2a, but using the wavelength of the NIST LaB_6 standard sample (SRM 660a)[S5] (ECH0005658, ID550625) for wavelength determination and the Rietveld-fit of the Cu reference powder recorded in the in situ setup for the determination of the zero-shift.

Attempt of size-strain-analysis of high resolution diffraction data[S6]

Size-strain analysis was carried out by the Williamson–Hall method on the high-resolution data. The peak widths obtained from the pattern decomposition procedure were corrected for the instrumental influences (instrumental broadening, Fig. S2). The used fitting function ("pseudo-Voigt 1") is a linear combination of a Gaussian and a Lorentzian component:

$$\left(\frac{2H}{\beta}\right)^{pV} = \left(\frac{\pi^{\frac{1}{2}}}{\left[2(ln2)^{\frac{1}{2}}\right]} + \left\{\frac{\pi}{2} - \pi^{\frac{1}{2}}/\left[2(ln2)^{1/2}\right] \cdot \eta\right\}\right)^{-1} \tag{1}$$

The integral breath of the pseudo-Voigt 1 is:

$$\beta_{pV} = \frac{\pi H/2}{\eta + (1-\eta)\sqrt{\pi \ln 2}} \tag{2}$$

Wherein β_{pV} is the integral breath of the scattered intensity, H is the FWHM and η is the profile shape factor ("Lorentz-Factor").

The Lorentzian contribution can now be calculated by

$$\frac{\beta_L}{\beta_{pV}} = b_0 + b_1\eta + b_2\eta^2 \tag{3}$$

with b_0=0.017475, b_1=1.500484 and b_2=-0.534156.

The Gaussian contribution is given by

$$\frac{\beta_G}{\beta_{pV}} = c_0 + c_{1/2}(1 + c\eta)^{1/2} + c_1\eta + c_2\eta^2 \tag{4}$$

with c_0=0.184446, $c_{1/2}$=0.812692, c_1=-0.659603 and c_2=0.44552.

Pattern decomposition according to this method works for 0.1≤ η ≤ 0.95 with a accuracy of 1%.[S7] Peaks with η=0 are treated as pure Gaussian, Peaks with η=1 as pure Lorentzian. Further information about the deconvolution procedure can be found in ref. [S?].
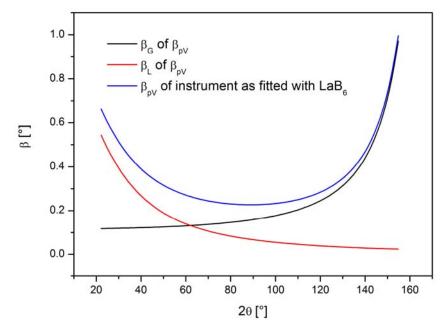

Figure S2: Instrumental contributions to the integral breadths as measured for the LaB$_6$ standard on ECHIDNA as a function of solid scattering angle in 2θ. The ratios of the corresponding Gaussian and Lorentzian components according to the fitted profile shape factor are marked in black and red color.

For the simplified integral breadth method by Williamson and Hall the instrumental broadening was subtracted from the observed scattering intensity of the Cu-Phase. The corrected breath of the scattering intensity was plotted versus 1/d according to the relationship:[S?]

$$\{\beta_{obs} - \beta_{inst}\}\cos\theta = \lambda/D_v + 4\,\varepsilon_{str}\{\sin\theta\} \tag{5}$$

The volume-weighted crystallite size D_v could be obtained from the y-intercept of a linear fit, while the slope gives the strain.
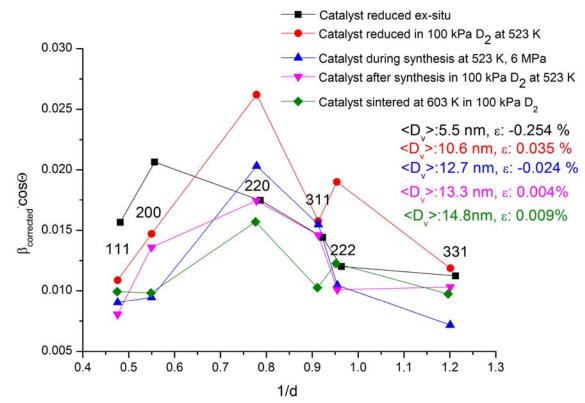

Figure S3: Williamson-Hall plot of the Cu/ZnO/Al$_2$O$_3$ catalyst at different states.

The experimentally determined Williamson-Hall-plot is shown in Figure S3. No linear behavior can be observed and this approach does not reveal a conclusive picture and seems inappropriate for this material. This is probably due to the high concentration of stacking faults, which has been detected in active $Cu/ZnO/Al_2O_3$ catalysts.[S8]aa